From the calculated and experimental data for samples with medium hydrogen content (H/Me=0.3-0.7) great discrepancy in the phonon density of states are observed. In this cases influence of different alloying elements is the dominant term in comparison with hydrogen-hydrogen interaction.

5.3.3 Modelling of low hydrogenated samples

In the system with low hydrogen content the approximation that hydrogen atoms are noncorrelated and oscillate around equilibrium point is valid. Hydrogen atom is in the force field from neighbouring metal atoms only. Interatomic potential could be described in the form [Fukai 1981]:

$$u(r) = Ae^{-\alpha R} \tag{5.7}$$

where R is metal-hydrogen distance and α describes the strength of potential. Expanding potential of nearest neighbors up to second term relation for the energy of hydrogen oscillation was obtained:

$$\Delta E = \frac{\hbar}{R}\sqrt{\frac{2A}{m}}\alpha R e^{-\alpha R/2}\sqrt{1-\frac{2}{\alpha R}}. \tag{5.8}$$

Using the relation [Fukai 1981] for short distance interaction with αR=40. The density of state could be obtained but without knowledge of the distribution of metal-hydrogen distances it is not possible. Due to alloying effects hydrogen atom are not located in the middle of octahedra, they have spatial distribution which in rough approximation can be described by Gaussian distribution. This assumption suppose a random distribution of hydrogen neighbourhood. For further calculations the estimation of half width full maximum of Gaussian is made. It will be used as a very rough assumption. Firstly we know for the Pd system with high and low hydrogen content: E_{high}/E_{low}=1.18 and R_{high}/R_{low}=0.93. Let assume this relation is also valid for the given system. Experimental data shows that this relation is in the first approximation valid. Using relation (4.1) for the potential calculates changing of hydrogen position due to different metal neighborhood. In approximation of relation (4.2) $A \sim E^2$. From this relation was obtained:

$$\frac{E_1^2}{E_2^2} = \frac{A_1}{A_2} = e^{-2\alpha\delta}. \tag{5.9}$$

Where δ is changing of distance due to different alloying elements. In the case of Cr and Fe it gave an estimation of δ $\sim$0.01Å. This assumption is very rough and it will be used only in simulation.

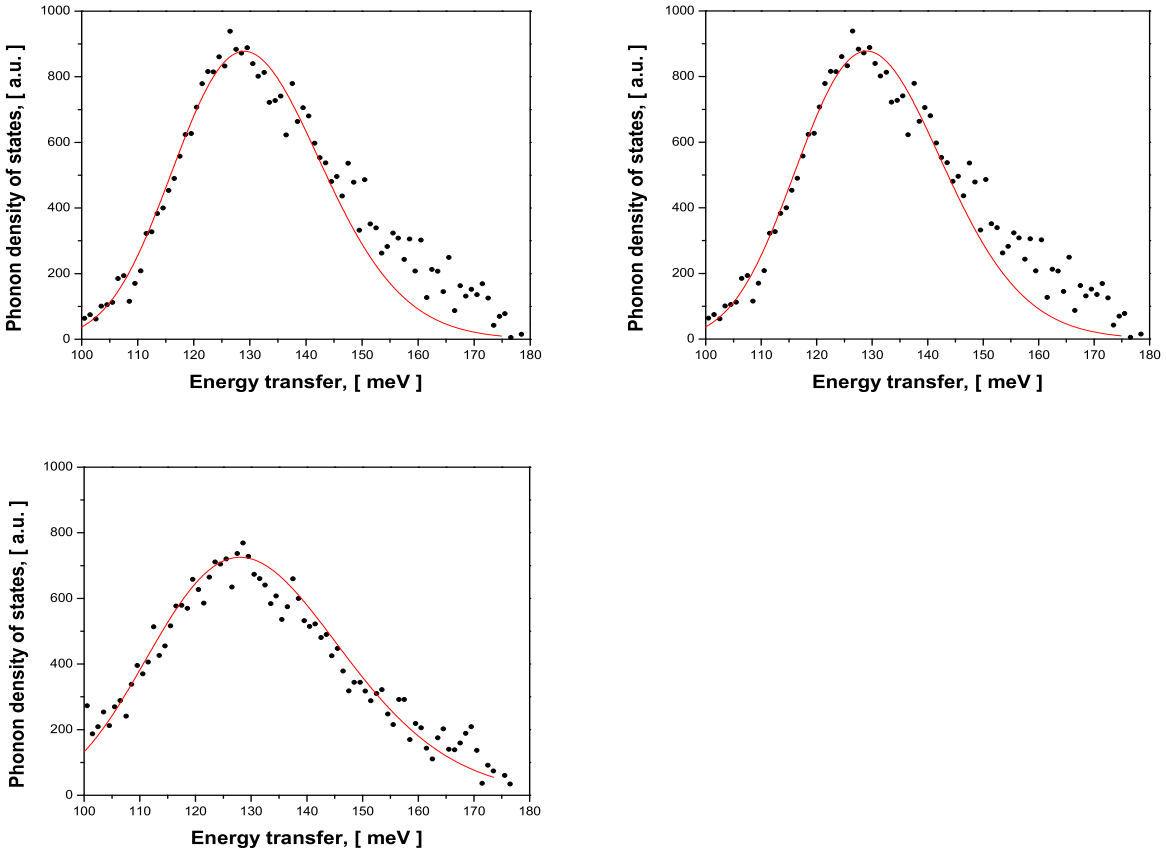

Figure 5.43: Phonon density of states for samples with 0.027 atomic % of hydrogen in austenitic stainless steel Fe-18Cr-16Ni-10Mn at different temperatures, T= 146, 194 ,246 K , • is experimental data and (—) model.

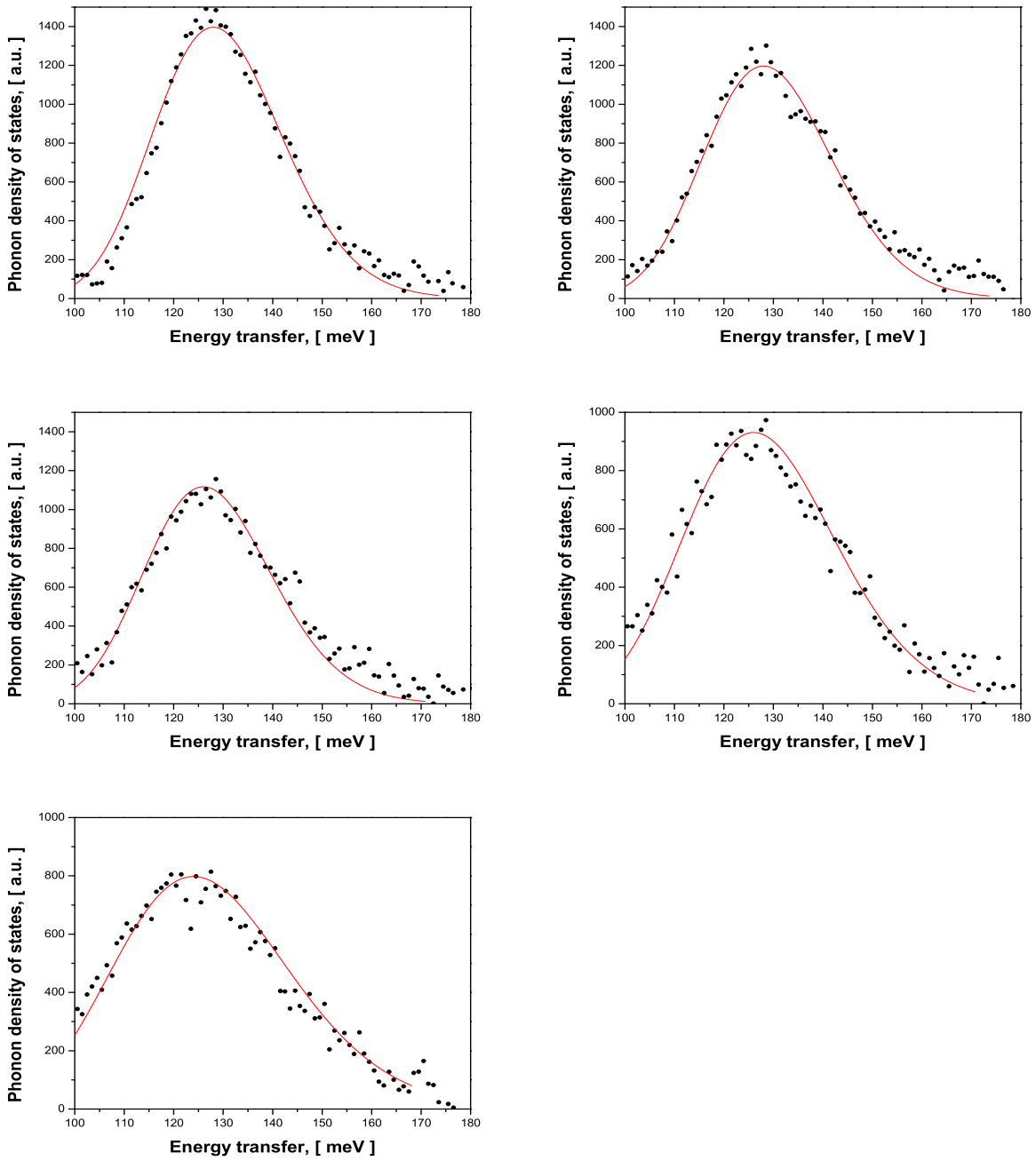

Figure 5.44: Phonon density of states for samples with 0.027 atomic % of hydrogen in austenitic stainless steel Fe-18Cr-16Ni-10Mn at different temperatures, T= 81, 147, 197 ,246 and 296 K respectively, • is experimental data and (—) model.

For medium hydrogen content its the hydrogen-hydrogen interaction is low we could treat it as a system of Einstein oscillators.

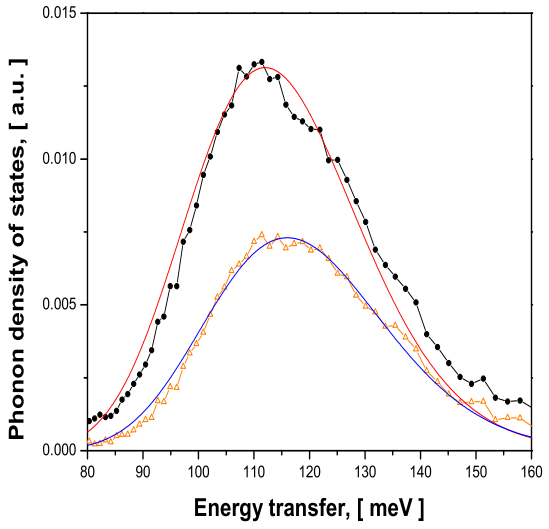

Figure 5.45: Simulation of phonon density of states for different hydrogen loading in hydrogenated austenitic stainless steel Fe-18Ni-10Cr, experimental data for (-●-) H/Me=0.56(5), H/Me=0.30(4) (-△-) and model calculation, (—) H/Me=0.56(5), H/Me=0.30(3) (—) respectively.

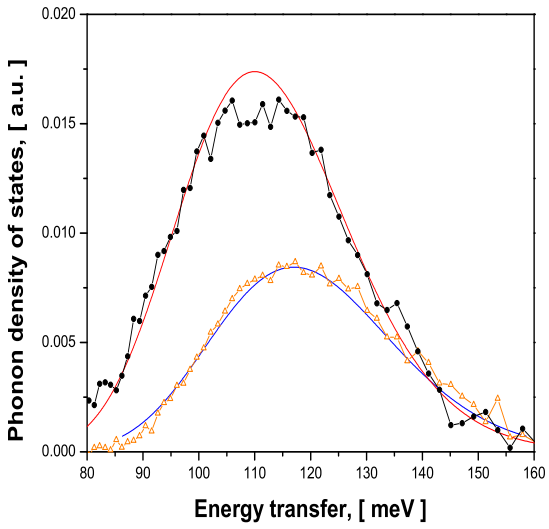

Figure 5.46: Simulation of phonon density of states for different hydrogen loading in hydrogenated austenitic stainless steel Fe-18Ni-10Cr, experimental data for (-●-) H/Me=0.66(3), H/Me=0.35(2) (-△-) and model calculation, (—) H/Me=0.66(3), H/Me=0.35(2) (—) respectively.

5.4 Conclusion

Based on the diffraction studies modelling of lattice dynamics was performed. The model Born-von Karman model with second neighbour shells was used. In the fully hydrogenated austenitic stainless steels hydrogenation has great impact on the acoustic modes. Due to the lattice expansion the acoustic frequencies are significantly lowered for about 1/3. Hydrogenation also changes the shape of the phonon dispersion curves. Due to a lack of reliable data a good comparison between theory and experiment is not possible. The calculated acoustic parts of the phonon dispersion curves are very similar to a very different system with rock-salt structure and great differences in the mass of the constituents, like: Pd-D and the UC system. These two systems are used for a comparison, because they present a limes for strong(Pd-D) and weak(UC) hydrogen-hydrogen interaction. It is also seen, that the weakening of the metal-metal force constants has only little influence on the optical modes.

The experimental data for highly hydrogenated austenitic stainless steels show significantly different results from the samples with medium and low hydrogen content. The fully hydrogenated samples have obviously a two peak structure (longitudinal, transversal) due to the hydrogen-hydrogen interaction. In the samples with medium and low hydrogen content only one non-symmetric peak exists. The dominant term in the samples is due to different alloying elements.
The results of the simulation of the lattice dynamics in fully hydrogenated austenitic stainless steels gave good agreement with the experiment, when both the H-H interaction and the influence of different alloying elements were taken into account. This simulation gave also values for the H-H force constants (table 5.5) similar to Pd-D system. The force constants obtained with the approach of [Rafizadeh 1981] were used for the simulation of the phonon dispersion curves, which agree pretty well with the experiment. These simulations fit much better to the experimental data for austenitic stainless steel Fe-18Cr-10Ni than for Fe-25Cr-20Ni. One of the reasons could be a very high amount of alloying elements.
In the case of low hydrogenated samples a simple model based on the Einstein oscillators describes the experimental data well (fig. 5.43, 5.44), only a slight disagreement in the high energy part exists. This disagreement is due to multiphonon processes as well as contributions from the background. As the free parameter the difference between the centre of octahedra and the real hydrogen positions was used. The obtained values showed a good agreement to the predicted values and they also slightly increase with temperature. This parameter is almost not influenced by the amount of hydrogen. The same model was applied on the samples with medium hydrogen content resulting in an excellent agreement (fig. 5.45, 5.46). The reason for this behaviour is a relatively low contribution of the hydrogen-hydrogen interaction to the lattice dynamics and the influence of the different alloying elements taken into account in the Born-von Karman model. The influence of the latter is not only described through the shift of the energy of the bonds, but also by the displacement of the hydrogen atoms from the centre of octahedra, which is the main contribution to the phonon density of states.

Chapter 6

Lattice dynamics in $Cu_{2-\delta}Se$

6.1 Diffraction studies

6.1.1 Experiment

Polycrystalline samples were prepared as follows. High purity copper and selenium powders were mixed in a suitable ratio and sealed under vacuum ($p < 10^{-5}$ mbar) in a silica tube. The mixtures were heated up to 720 K for about 100 hours with a subsequent annealing for 48 hours at 420-520 K. After slow cooling to room temperature the powders were ground and then homogenised under vacuum for 100 hours at 670 K.
Neutron, X-ray and synchrotron powder diffraction measurements[9] have been performed with $Cu_{2-\delta}Se$(δ=0;0.15;0.20;0.22;0.25) compounds at room temperature and at elevated temperatures up to 623 K. Neutron powder diffraction measurements were performed with DN-2 multipurpose diffractometer at IBR-2 reactor (JINR, Dubna). Synchrotron diffraction measurements were performed using the high resolution synchrotron powder diffractometer at the B2 beamline at HASYLAB (Hamburg) with the on-site readable image plate scanner (OBI).
The X-ray powder diffraction patterns at room temperature were collected on a STOE STADI P, equipped with a linear position sensitive detector with 6° aperture. A curved Ge (111) monochromator was used to select $CoK_{\alpha 1}$ radiation. Diffraction patterns have been collected in the range of 10-120° with steps $\Delta(2\delta)$=0.02 °. synchrotron measurements at elevated temperatures were performed at the B2 powder diffractometer at HASYLAB with two compositions, Cu_2Se and $Cu_{1.85}Se$. The samples were heated using a STOE capillary furnace. Diffraction patterns have been collected in the range 10-90° in steps 0.004° using photons with wavelength 0.708785 Å, selected by a Si (111) double crystal monochromator. All data were analysed with the Rietveld software package FullProf [Fullprof 2002].

[9] experiments were performed by Andrei Skomorokhov and Michael Knapp

6.1.2 Results

Average structure

The structure model as proposed in [Rahlfs 1936] (space group $Fm\overline{3}m$) was used for Rietveld refinements. As discussed above, Se atoms are situated in 4a site, where copper atoms are distributed over 8c and 4b sites. After that disorder of copper atoms was introduced by splitting 8c and 4b sites. In the refinements vibration of copper and selenium atoms are supposed to be isotropic. The Rietveld refinements show a low amount of copper atoms in octahedral voids for $Cu_{1.75}Se$, $Cu_{1.78}Se$ and $Cu_{1.8}Se$ at room temperature and no copper atoms in octahedral voids for samples: $Cu_{1.85}Se$ and Cu_2Se at elevated temperature. One possible explanation for the absence of copper atoms in octahedral voids is higher coulomb repulsion. When a copper ion is located in an octahedral position, its distance to other copper ions in tetrahedral voids is smaller than the distance to selenium ions. Therefore the presence of Cu ions in octahedral voids is energetically less favorable. This effect is more pronounced for samples with higher concentration of copper ions.

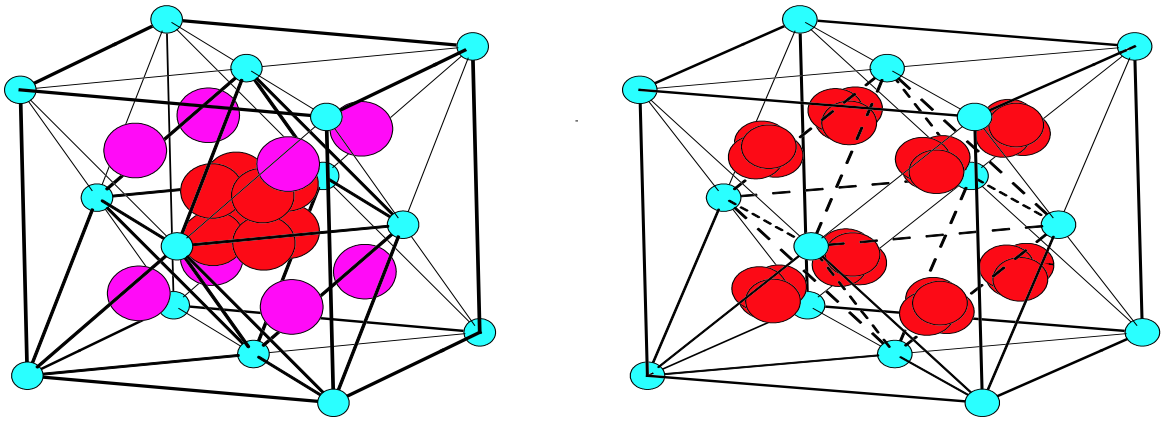

Figure 6.1: The structural models for copper ions distribution in $Cu_{1.75}Se$, $Cu_{1.78}Se$, $Cu_{1.8}Se$ (left side) and Cu_2Se, $Cu_{1.85}Se$ (right side). Selenium atoms are shown by small spheres and copper with larger one.

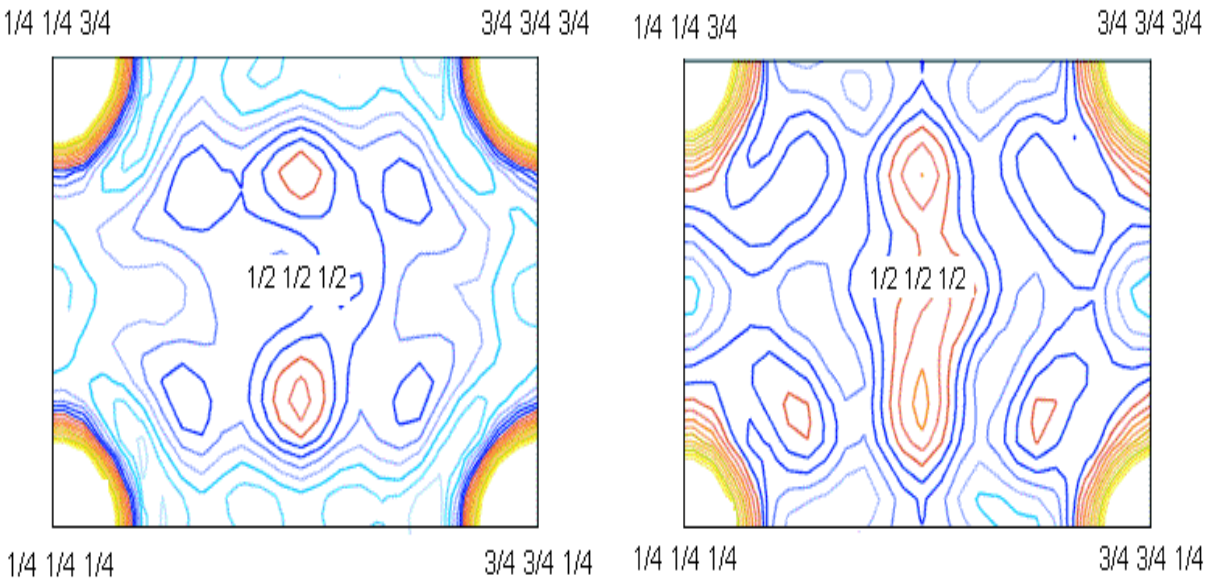

Figure 6.2: Fourier maps of the electron density in the (011) plane within tetrahedral sites in $Cu_{1.75}Se$ at room temperature and Cu_2Se at T=423 K. Contours are drawn at intervals of 1e/Å.

Models in (fig. 6.1), describe the average structure in $Cu_{2-\delta}Se$. Assuming the accepted conductivity mechanism of Cu atoms moving along the space diagonal from one tetrahedral cavity over an octahedral cavity to other tetrahedral, it is interesting that no occupation of octahedral sites can be observed in Cu_2Se and $Cu_{1.85}Se$.When δ is increased also the average distance of copper ions from the centre of octahedra is increased. The same behaviour of copper ion distribution is also observed for the copper ions which are located in tetrahedral intersitial sites. Similar results have been reported in other fcc-based superionic conductors like CuI, Ag_2Te and Cu_2S [Sakuma 1989, Keen 1998, Keen 1995]. A different distribution of copper ions in α-$Cu_{2-\delta}$ have been reported in [Heyding 1976, Yamamoto 1991] which is in contradiction to our results. The diffusion pathway is clearly seen in (fig. 6.2), where Fourier map of electron density in (110) plane is constructed for Cu_2Se and $Cu_{1.75}Se$ at room temperature. This construction was performed using GFOURIER, which is additional package of Fullprof [Fullprof 2002]. Dynamics of diffusion processes could not be determined with X-ray powder diffraction.

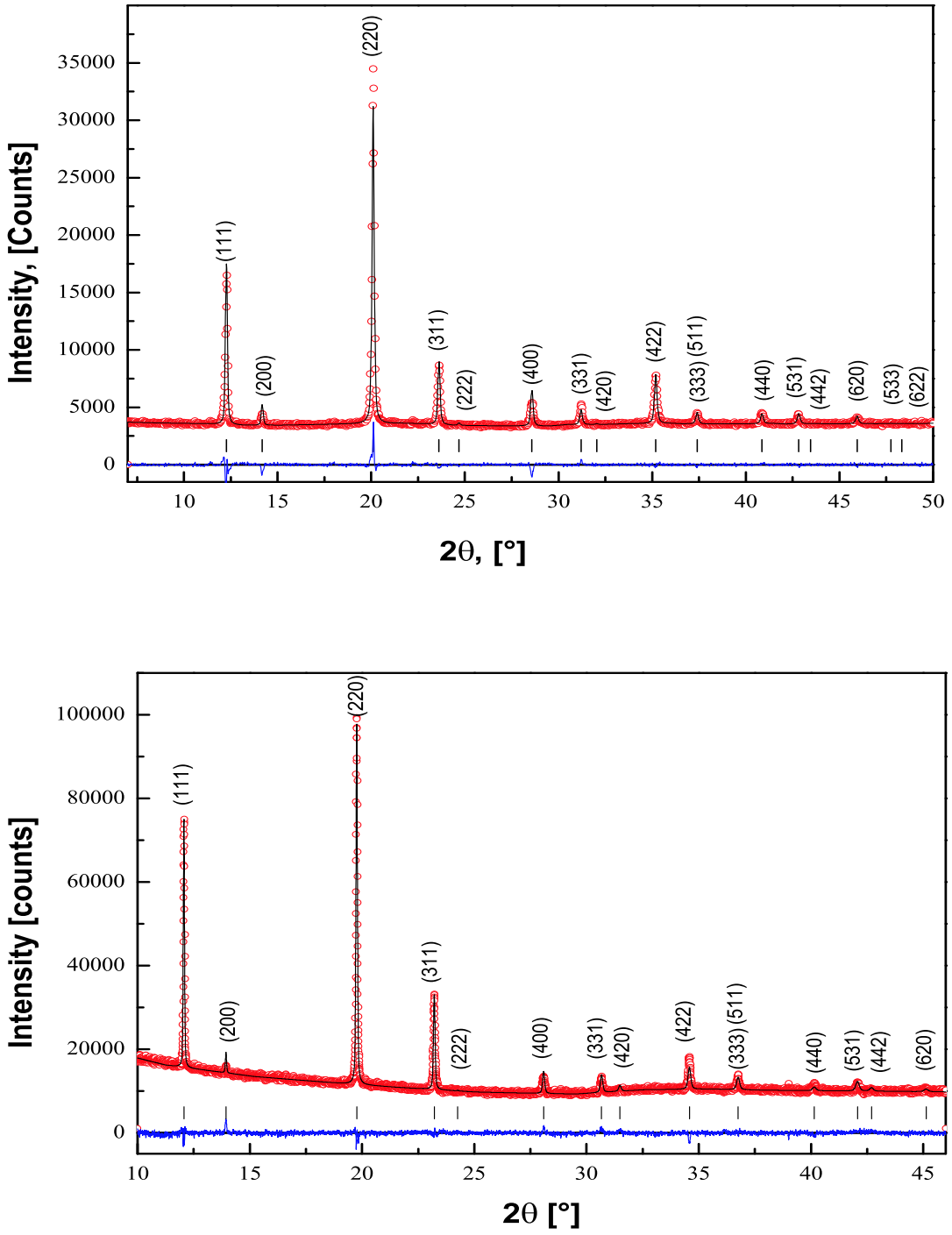

Figure 6.3: Observed, calculated and difference X-ray(up) and synchrotron(down) powder diffraction pattern of $Cu_{1.75}Se$ (RT) and Cu_2Se (T=423 K).

Table 6.1: Summary of the results of the Rietveld refinements, based on diffraction data collected for $Cu_{1.75}Se$, $Cu_{1.78}Se$, $Cu_{1.8}Se$, $Cu_{1.85}Se$ and Cu_2Se.

Comp.	$Cu_{1.75}Se$		$Cu_{1.78}Se$	$Cu_{1.8}Se$	$Cu_{1.85}Se$		Cu_2Se
Temp.	RT	423 K	RT	RT	423 K	583 K	423 K
a(Å)	5.7478(1)	5.7624(1)	5.7464(1)	5.7542(1)	5.7932(2)	5.8165(2)	5.8413(2)
Se 4a(000)							
Occ.	4	4	4	4	4	4	4
B_{iso}(Å^2)	3.1(9)	4.9(9)	4.6(9)	4.5(9)	1(1)	2(2)	1(1)
Cu 8c($\frac{1}{4}\frac{1}{4}\frac{1}{4}$)							
Occ.	6.1(2)	6.1(5)	6.5(2)	6.5(1)	0	0	0
B_{iso}(Å^2)	2.7(5)	4.6(5)	5.4(5)	4.6(5)			
Cu 32f(xxx)							
Occ.	0.9(2)	0.9(5)	0.6(2)	0.7(1)	7.4	7.4	8
x	0.415(8)	0.378(4)	0.407(8)	0.411(4)	0.282(5)	0.292(5)	0.291(5)
B_{iso}(Å^2)	2.7(5)	7.6(5)	5.4(5)	4.6(5)	4.2(8)	5(5)	4.9(8)
Bragg R-fac.	2.98	1.19	2.44	4.22	5.64	11.0	10.6

Copper releasing process

Copper releasing process from stoichiometric α-Cu_2Se has been observed at elevated temperature (573 K) by synchrotron diffraction. On heating copper segregates from stoichiometric Cu_2Se compound with changes of composition and decrease of the lattice parameter. Temperature evaluation of the peak with highest intensity (220) in $Cu_{2-\delta}Se$ between 423 and 593 K is shown in (fig. 6.4). It is clearly seen that at T = 573 K the peak has a doublet structure in contrast to T =423 and 593 K. A doublet structure corresponds to a phase mixture. This mixture is composed of two fcc phases with lattice parameters of a = 5.85(1) and 5.82(1) Å. During the first measurement the fraction of the phase with a = 5.85 Åwas 71%, while during the second it was only 18%. From this we could conclude that time of measurement is similar to time of phase transition. At 593 K the lattice parameter of Cu_2Se compound is very close to the lattice parameter of $Cu_{1.85}Se$. This is an indication that about 7 at. % of copper is released from Cu_2Se at 593 K. The diffraction pattern of Cu_2Se at T = 573 K in a whole range is shown in (fig. 6.4). Copper releasing process observed in our experiment could be important to understand the average structure in α-Cu_2Se.

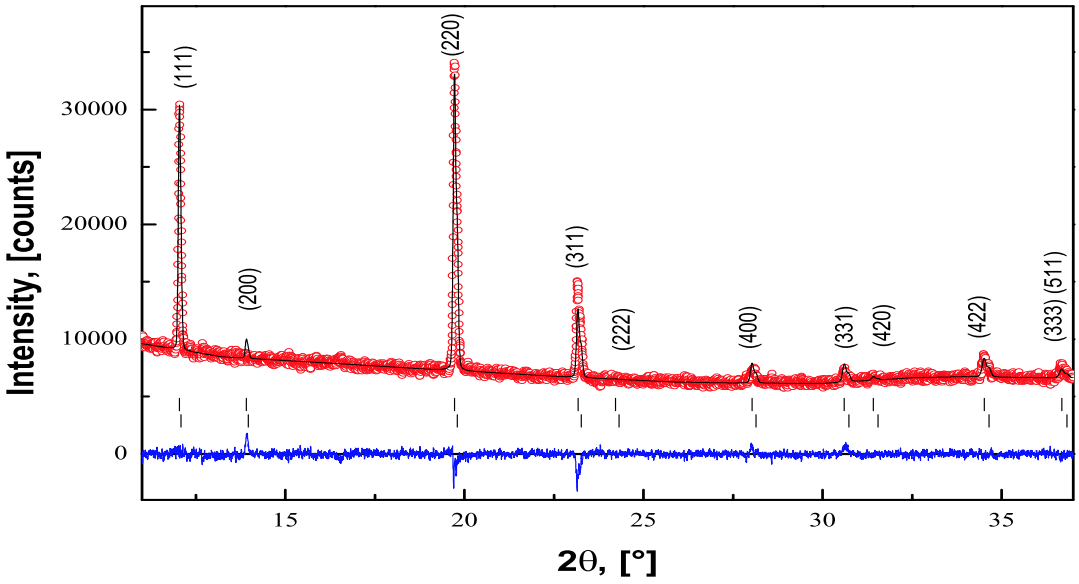

Figure 6.4: The least-squares fit to the powder synchrotron diffraction data(λ=0.70878 Å) of Cu_2Se sample at 573 K. The upper and lower rows of ticks correspond to the Bragg reflections of space group with lattice parameters a= 5.85(1) and 5.82(1) Å respectively.

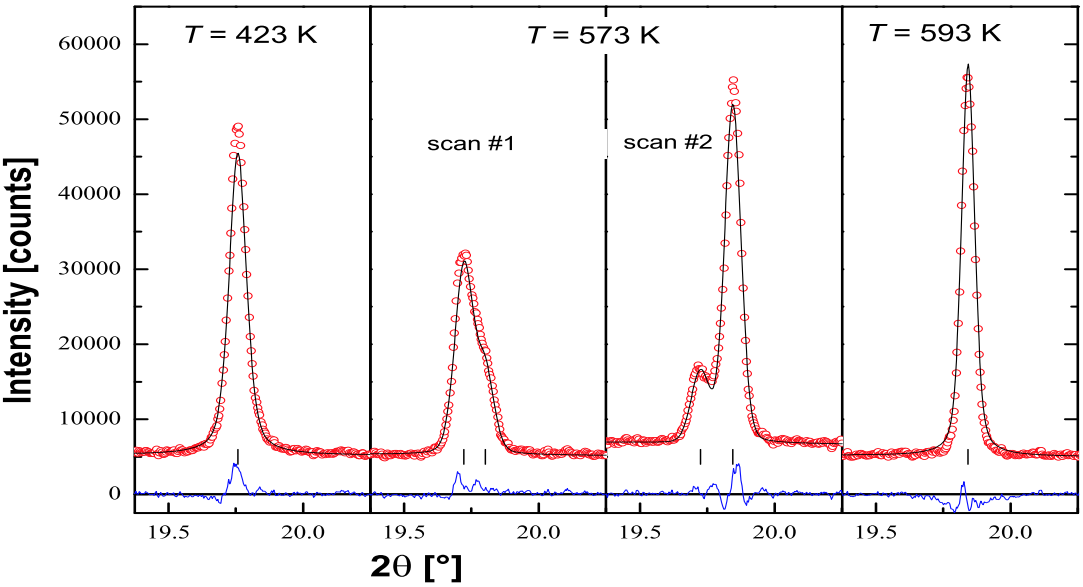

Figure 6.5: Evaluation of the (220) Bragg reflection with temperature.

6.1.3 Conclusion

The structure in α-copper selenide is determined as a function of composition . In $Cu_{1.75}Se$, $Cu_{1.78}Se$ and $Cu_{1.8}Se$ at room temperature the cations occupy tetrahedral and octahedral interstices within the fcc anion sublattice. In $Cu_{1.85}Se$ and Cu_2Se at elevated temperature no octahedral occupation has been detected, although considerable copper density is localised near the tetrahedral-octahedral boundary. It is suggested that the cations diffuse in a skewed <111> direction via the periphery of octahedral voids. For the more accurate data about process of diffusion quasielastic neutron scattering is required. The phase diagram of the system Cu-Se is not completely determined yet, especially on the low and high temperature regions. Diffraction studies gave indication that exsolution of copper in copper selenide occurs. In the diffraction pattern copper reflections are not observed, one of the reason of this effect might be the very small size of copper grains. To prove the exsolution of copper it is necessary to perform EDX studies at elevated temperatures.

6.2 Inelastic neutron scattering

6.2.1 Experiment

Inelastic neutron scattering measurements[10] with polycrystalline samples were carried out with the time-of-flight spectrometer DIN-2PI (Dubna) at an incident neutron energy of 12.3 meV. Samples of about 50 g were placed in a cylindrical container made from a thin aluminium foil. Neutron scattering spectra were collected simultaneously at 15 scattering angles in the range 28-133°. The energy transfer was from -9 meV to about 160 meV (negative values correspond to neutron energy loss). The energy resolution was 0.83 meV full width at half maximum in elastic scattering. The raw data were corrected for background, detector efficiency and scattering from the container. Finally, the dynamic structure factor $S(Q,\omega)$ and frequency distribution $g(\omega)$ were obtained from the time-of-flight spectra.
Phonon dispersion curves on a single crystal of $Cu_{1.85}Se$ were measured with the triple-axis spectrometer UNIDAS, FZ Jülich. A crystal with lattice parameters 5.752(2) Å and mosaic spread about 30' was aligned with (011) as scattering plane. Constant Q-mode was used with fixed wavelength of the incident neutrons. We used two fixed wavelengths (λ = 2.355 and 4.087 Å).

6.2.2 Result

Density of states in $Cu_{2-\delta}Se$

Dynamical structure factor $S(Q,\omega)$in Cu_2Se and $Cu_{1.75}Se$ at room temperature have a similar structure and consist of three components (fig. 6.8). The first one is a elastic peak which has the highest intensity. The width of this component corresponds to the instrumental resolution. The second component is the broad peak with much lower intensity

[10]experiments were performed by Andrei Skomorokhov

which is also centered around the elastic line. The width of this peak is about 2-6 meV. and it is nearly independent on Q. This peak correspond to the quasielastic neutron scattering. Precise determination of parameters of the broad peak is disabled by the presence of the third component in the spectra - intensive LE - mode in energy interval of 3-4 meV. Nevertheless a large width and a weak Q - dependence of the broad peak suggest a localised motion of about 0.3-0.8 ps. The LE - peak in Cu_2Se and $Cu_{1.75}Se$ show strong Q - dependence of the intensity, while the energy of the LE - excitation is nearly constant for different scattering angles. The peaks with the highest intensity have a smaller width and they are located near Q $\sim$ 3.1 $\mathring{A}^{-1}$. This value is close to the position of the elastic coherent Bragg reflection from the (220) plane. With increasing difference in wave vector for LE mode to 3.1 $\mathring{A}^{-1}$, its intensity decreased and width increased. Such dependence on Q is characteristic for inelastic scattering for LE phonons with small wave vectors $\vec{q}$. The condition for one phonon coherent scattering ($E_i - E_f = \pm\hbar\omega$) and ($2\pi\tau_{hkl\pm} = Q$), where E_i and E_f are the energies of incident and scattered neutrons.

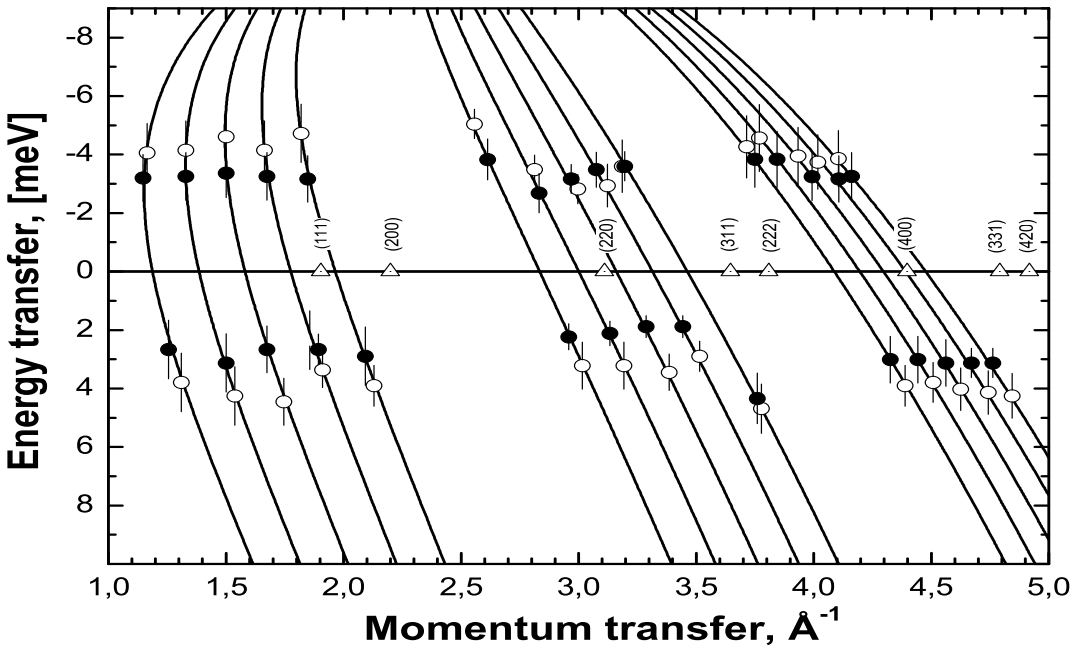

Figure 6.6: The position of LE- peaks for α - $Cu_{1.78}Se(\circ)$ and β - $Cu_2Se(\bullet)$. Lines correspond to kinematical low for 15 scattering angles used in the experiment, $\triangle$ denote the position of Bragg reflections.

First we note that S(Q,ω) of these compounds do not differ much (fig. 6.8) although α -$Cu_{1.78}Se$ is in the superionic state. Low- energy modes exist in both compounds. Intensity and energies of LE-peaks are slightly higher for $Cu_{1.78}Se$ (Average energy of the LE peaks

are 3.9 meV for $Cu_{1.78}Se$ in comparison with 3.5 meV for β-$Cu_{1.78}Se$, (fig. 6.7). The Q - dependence of the LE- energy mode is also similar for $Cu_{1.78}Se$ and Cu_2Se (fig. 6.8).

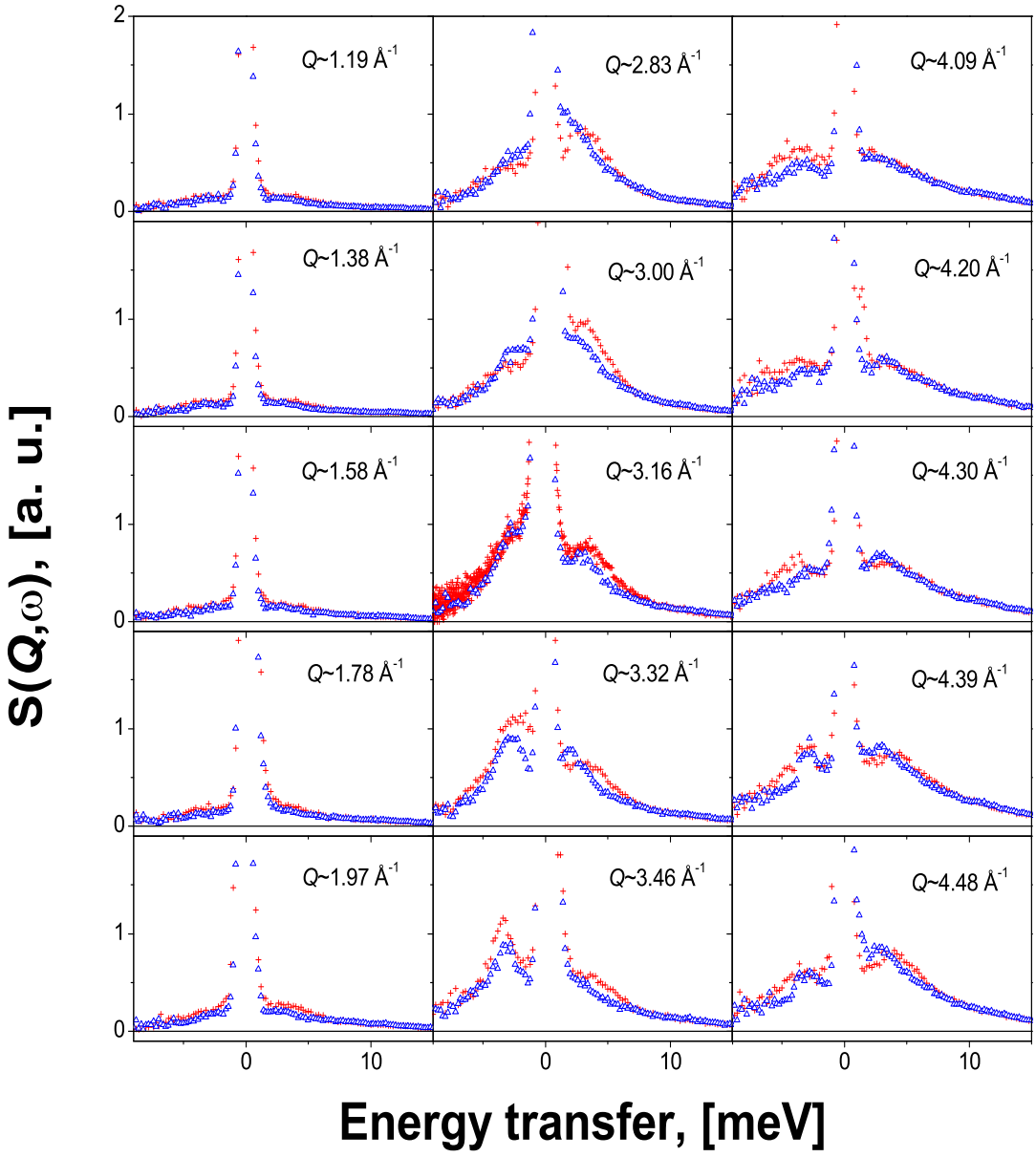

Figure 6.7: Dynamical structure factor of α -$Cu_{1.78}Se$(+) and β -Cu_2Se(△). Wave vector of the spectra correspond to the value of elastic scattering.

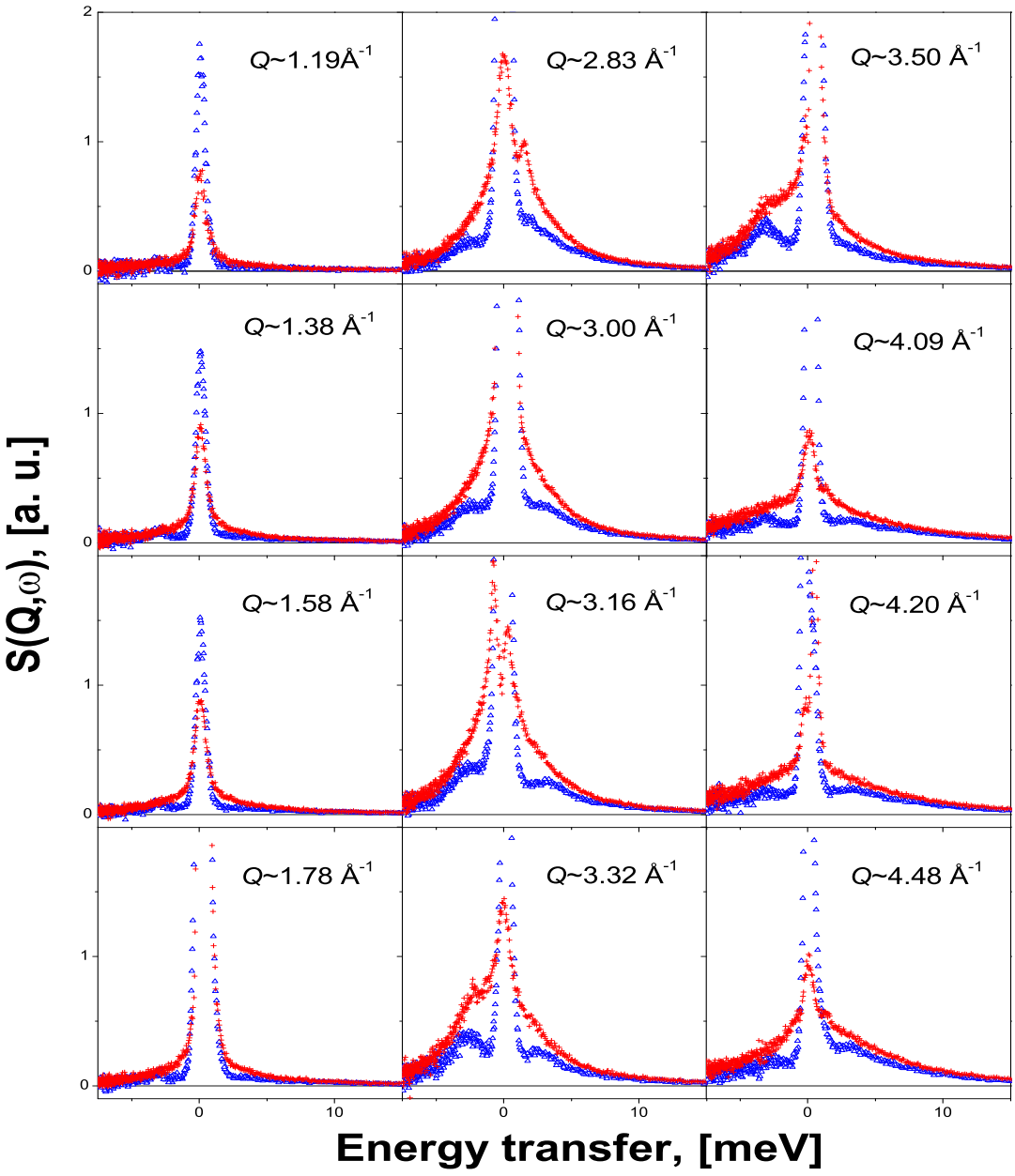

Figure 6.8: Dynamical structure factor of α -Cu_2Se(+) and β -Cu_2Se(△). Wave vector of the spectra correspond to the value of elastic scattering.

Experimental phonon density of states, calculated multiphonon contribution and derived one- phonon density of states are shown in (fig. 6.9). Multiphonon intensity was calculated by an iterative procedure as described in [Dawidowski 1998, Dawidowski 2002]. Weight

and line shape of the one-phonon process as well multiphonon intensity depends very much on values of the Debye-Waller exponent. Therefore for precise multiphonon correction preliminary knowledge of the Debye-Waller factor is desirable. However iterative procedure described in [Dawidowski 1998, Dawidowski 2002] allow us to perform calculation of the multiphonon component as well to determine the Debye-Waller factor. Reliability of this calculation depends on completeness of frequency range g(ω) measured in experiment and accuracy of experimental data. Measured interval of frequency distribution in $Cu_{2-\delta}Se$ during experiment was up to 160 meV whereas boundary of the lattice vibration in the copper selenide system is about 30-35 meV. Mean square displacement of the atoms in Cu_2Se at T=423 K is higher than in $Cu_{1.75}Se$ and Cu_2Se at room temperature region. A significant difference exist between density of states for different samples. Phonon density of states in non-superionic Cu_2Se at room temperature could be described roughly as a sum of four contributions: low-energy peak centred at 3.5 meV, weakly pronounced peak at 8-9 meV overlapped with more intense peak at 12 meV and high energy peak at 22-24 meV. Peaks at 8 and 12 meV correspond to transversal and longitudinal acoustic phonons respectively. Peak at 22-26 meV correspond to optic vibrations in copper selenide. Low energy peak is characteristic low-energy mode with intensive low-energy peaks in $S(Q, \omega)$. In $Cu_{1.75}Se$ at room temperature changes of the phonon density of states are rather big. Only three peaks could be distinguished in $g(\omega)$ of $Cu_{1.75}Se$: low-energy peak at 5-7 meV, acoustic peak at the 12 meV and optic peak at 22-24 meV. Key point is increasing of the intensity of the low-energy peak. Analysis shows that intensity of the low-energy peak increased four time and it is centred in $Cu_{1.75}Se$ at higher energy than in Cu_2Se. Phonon density of states in Cu_2Se at T=433 K differs from $g(\omega)$ in Cu_2Se and $Cu_{1.75}Se$ at room temperature. Low energy mode was observed in $g(\omega)$ for all three samples.

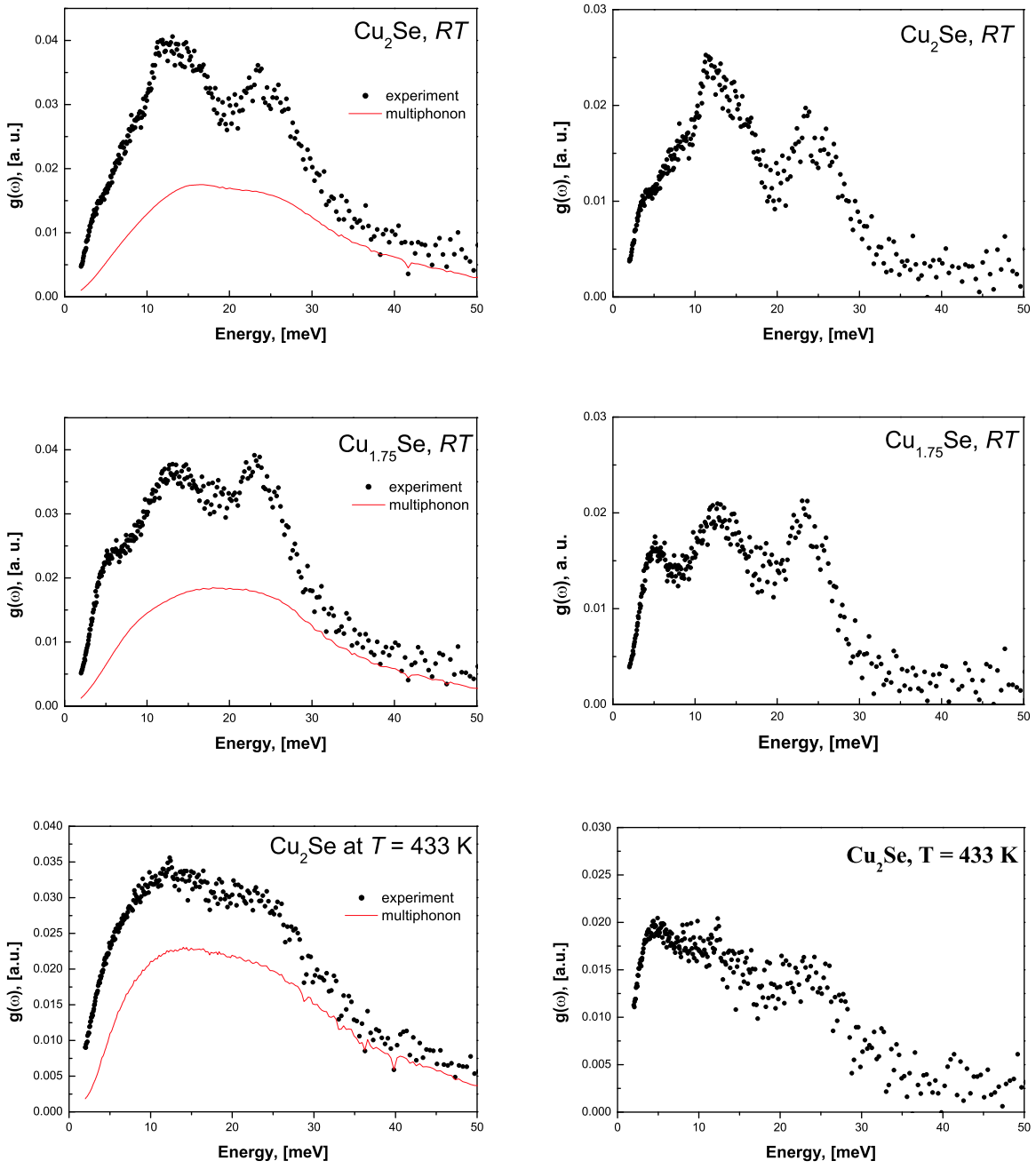

Figure 6.9: At the left side of picture are experimental generalised frequency distribution and multiphonon contribution of Cu_2Se, $Cu_{1.75}Se$ at room temperature and Cu_2Se at 433 K. On the right side are corrected single phonon density of states.

Thermal properties

From $g(\omega)$, thermal properties(U, c_V, $< \Delta x^2 >$) can be calculated.

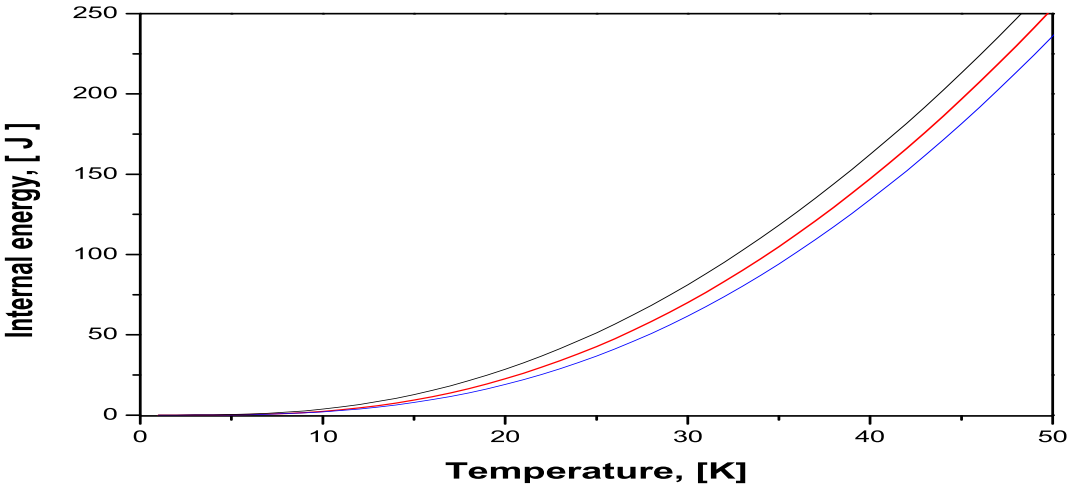

Figure 6.10: Internal energy for superionic and non-superionic phase of copper selenide calculated from $g(\omega)$ of (—)Cu_2Se, (—)$Cu_{1.75}Se$ at room temperature and (—) Cu_2Se at 433 K.

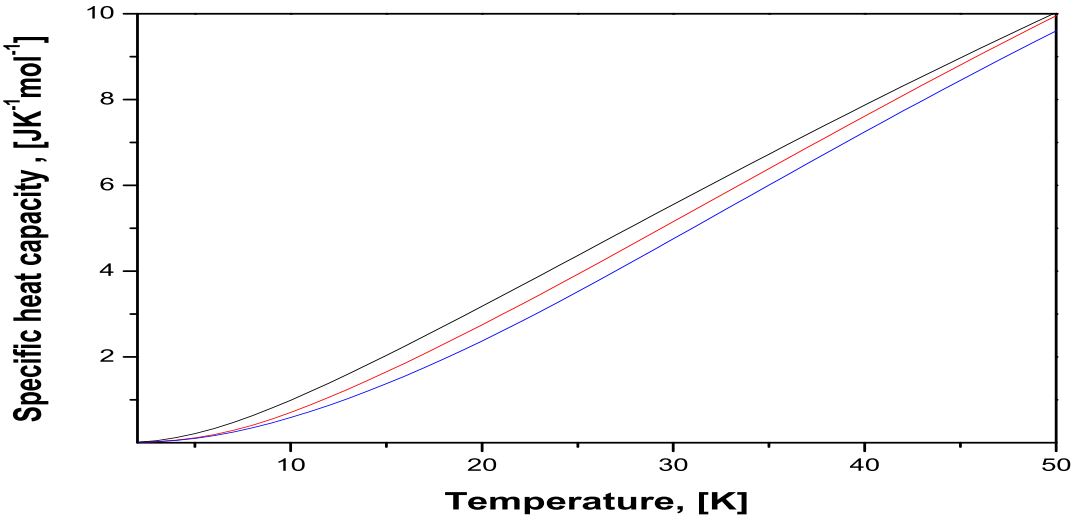

Figure 6.11: Specific heat capacity for superionic and non-superionic phase of copper selenide calculated from $g(\omega)$ of (—)Cu_2Se, (—)$Cu_{1.75}Se$ at room temperature and (—) Cu_2Se at 433 K.

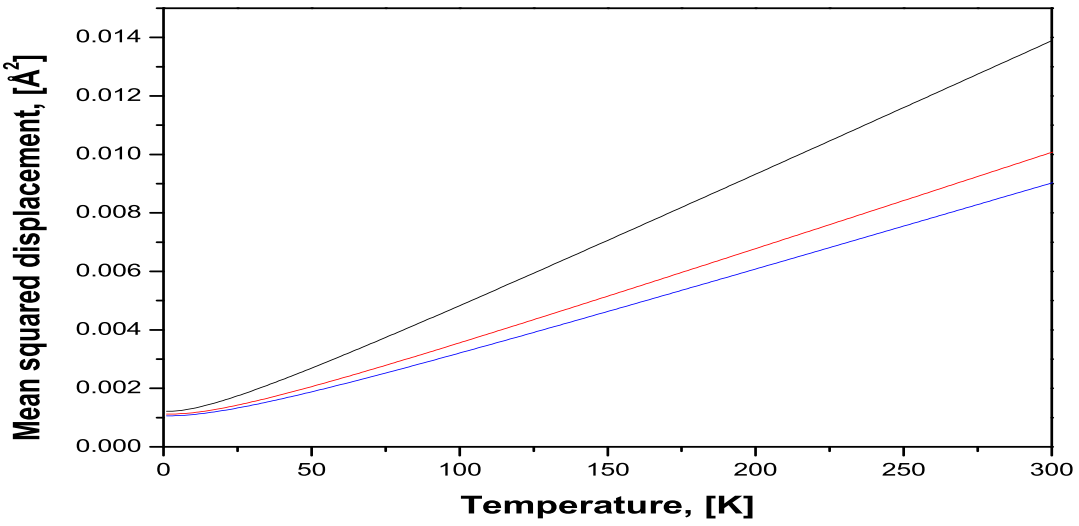

Figure 6.12: Mean atomic square displacement for superionic and non-superionic phase of copper selenide calculated from $g(\omega)$ of (—)Cu_2Se, (—)$Cu_{1.75}Se$ at room temperature and (—) Cu_2Se at 433 K.

Dispersion relation in α-$Cu_{1.85}Se$

Dispersion relation in α-$Cu_{1.85}Se$ single crystal in high symmetry directions([100], [011] and [111]) have been measured (fig. 6.13). In the direction [011] only one of two transverse modes was measured. The measured phonon demonstrate a strong increase of the width with increasing reduced wave vector q and became extremely broad for q >0.4. This is the main reason why the dispersion curves near the Brillouin zone boundary were not observed. As seen from (fig. 6.13), all TA branches change the slope drastically and they became nearly flat at q >0.2-0.4 with an energy about 4 meV. This behaviour of transversal acoustic modes reflex in $S(Q,\omega)$ as LE peak(fig. 6.5). This also correlates with Q dependence of intensity of the LE - peaks in $S(Q,\omega)$ spectra (fig. 6.6). In contrast to transversal branches, the longitudinal phonons in [100] direction have a linear dependence on q up to a rather high value of the phonon wave vector. Damping of TA phonons, which appeared in our measurements in broadening of the phonon peaks, indicate a strong coupling of acoustic phonons with the motion of mobile ions. Error bars on the figure 6.13 correspond to estimated full width half maximum.

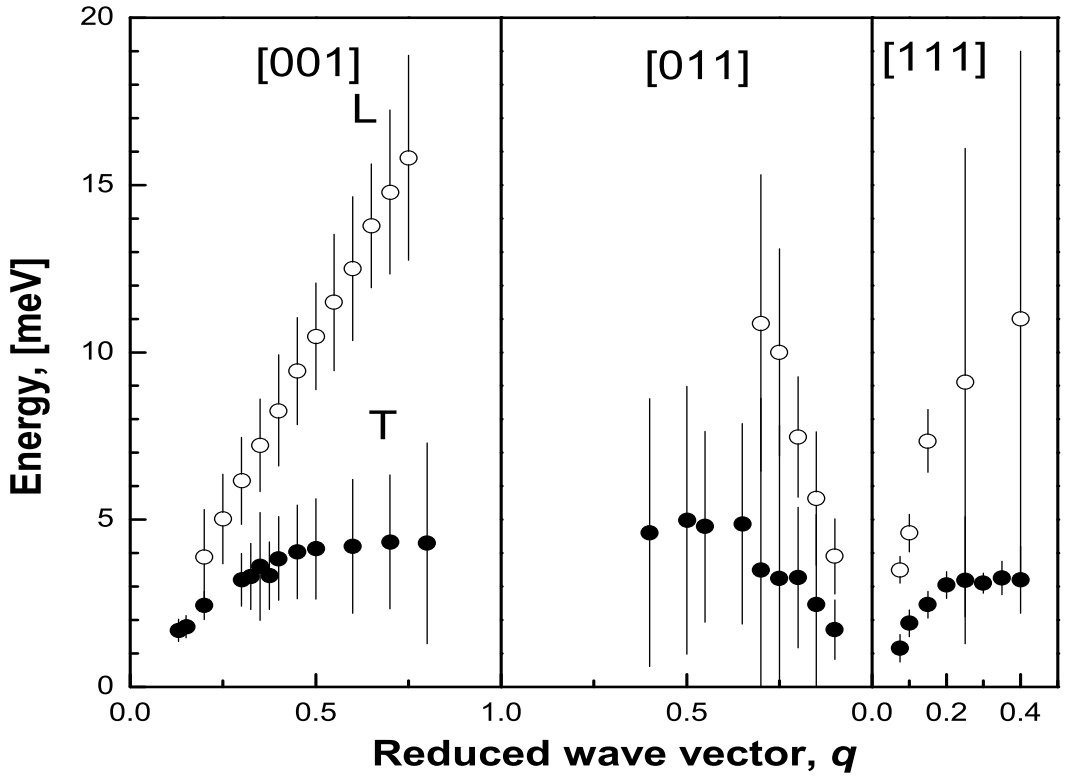

Figure 6.13: Dispersion relation in α-$Cu_{1.85}Se$. Vertical lines show the width of the phonon peaks.

6.2.3 Conclusion

The dynamic structure factor $S(Q,\omega)$ of $Cu_{1.78}Se$ and Cu_2Se in addition to elastic peak consist of the broad quasielastic component and LE - excitations with frequencies of 3.5-4 meV. We suggest that the broad component could be connected with fast-localised diffusion of Cu ions between split 32f sites. Intensity of LE-mode depends strongly on the scattering angle showing that LE-mode is related to the acoustic phonons. The TA dispersion curves of α-$Cu_{1.85}Se$ change drastically the slope and became dispersionless at q >0.4. Damping of phonons indicates the strong coupling of acoustic phonons with the motion of mobile ions. Further INS studies are necessary on α-$Cu_{1.85}Se$ due to total lack of knowledge on optic modes. Optic mode should be observed in the energy range between 20-30 meV, this assumption was based on experimental data for phonon density of states. Also should be performed realistic modelling which should confirm already measured DOS as well as dispersion curves.